rheumato

MDPI

Article

Development of NOD-DR3 as the Spontaneous Humanized Mouse Model for Sjögren's Disease

Alexandria Voigt [1], Shivai Gupta [1,†], Patricia Glenton [1], Verdugo Daniel [2], Danmeng Li [1] and Cuong Q. Nguyen [1,3,4,*]

[1] Department of Infectious Diseases and Immunology, College of Veterinary Medicine, University of Florida, Gainesville, FL 32608, USA; shivai.gup@gmail.com (S.G.); glenton@ufl.edu (P.G.); danmeng1986@ufl.edu (D.L.)
[2] Department of Comparative, Diagnostic & Population Medicine, College of Veterinary Medicine, University of Florida, Gainesville, FL 32608, USA
[3] Department of Oral Biology, College of Dentistry, University of Florida, Gainesville, FL 32608, USA
[4] Center of Orphaned Autoimmune Diseases, University of Florida, Gainesville, FL 32608, USA
* Correspondence: nguyenc@ufl.edu; Tel.: +1-352-294-4180; Fax: +1-352-392-9704
† Current address: Weave Bio, 575 Market Street, Suite 1300, San Francisco, CA 94105, USA.

Abstract

Background: Sjögren's disease (SjD) is a chronic autoimmune disorder characterized by lymphocytic infiltration of exocrine glands, leading to secretory dysfunction. While conventional mouse models have advanced understanding of disease mechanisms, translational limitations exist due to differences in immune system components, particularly MHC molecules. The NOD-DR3 mouse strain, expressing human HLA-DR3, a prominent genetic risk factor for SjD, offers a humanized model that has not been previously characterized for SjD phenotypes. Objective: To comprehensively characterize NOD-DR3 mice as a novel humanized model for SjD, evaluating functional, serological, histological, and immunological disease features with particular focus on sex dimorphism. Methods: Aged NOD-DR3 mice (20–32 weeks) were assessed for salivary flow rates, autoantibody profiles (ANA, anti-Ro52, anti-Ro60, anti-La), glandular focal scores, and immune cell infiltration patterns. Comparisons were made with established SjD models (NOD-*Aec1/2*, NOD) and healthy C57B6/J controls, with sex-stratified analyses. Results: NOD-DR3 mice exhibited significantly reduced salivary flow rates, comparable to those in established models. Seventy percent were ANA-positive, with pronounced sex-dependent patterns: males showed higher ANA frequency with nucleolar patterns, while females displayed elevated anti-Ro/La antibodies with speckled patterns. Notably, NOD-DR3 demonstrated the most severe lacrimal gland infiltration among all strains. Cellular analysis revealed striking sex dimorphism, with females showing 12-fold higher B-cell infiltration and enhanced Th17 responses, while males exhibited elevated macrophage and Th1 profiles. Conclusions: NOD-DR3 mice recapitulate cardinal SjD features with robust sex dimorphism, establishing this humanized model as a valuable translational platform for investigating HLA-restricted disease mechanisms and evaluating therapeutic interventions.

Keywords: Sjogren's disease; animal model; NOD-DR3; humanized mouse model

Check for updates

Academic Editor: Kenneth Pritzker

Received: 25 June 2026
Revised: 9 September 2026
Accepted: 29 September 2026
Published: 19 October 2026

Copyright: © 2026 by the authors. Licensee MDPI, Basel, Switzerland. This article is an open access article distributed under the terms and conditions of the Creative Commons Attribution (CC BY) license.

1. Introduction

Sjögren's disease (SjD) is a chronic systemic autoimmune disorder characterized by lymphocytic infiltration of exocrine glands, leading to progressive glandular dysfunction.

The hallmark clinical manifestations include keratoconjunctivitis sicca and xerostomia, resulting from secretory dysfunction of the lacrimal and salivary glands [1]. Beyond these sicca symptoms, patients frequently present with extraglandular manifestations, including arthralgias, vasculitis, peripheral neuropathy, and debilitating fatigue [2]. The disease exhibits a striking female predominance, with women affected approximately nine times more frequently than men, underscoring the critical role of sex-specific factors in disease pathogenesis [3]. Serologically, SjD is characterized by the presence of autoantibodies, particularly antinuclear antibodies (ANAs) and antibodies against the ribonucleoproteins Ro/SSA (Ro52 and Ro60) and La/SSB, which serve as important diagnostic markers and reflect the underlying breakdown of immune tolerance [4]. The precise etiology and pathogenic mechanisms driving SjD remain incompletely understood. The disease is recognized as multifactorial, involving complex interactions between genetic susceptibility, environmental triggers, hormonal influences, and dysregulated immune responses. The infiltration of T and B lymphocytes into exocrine glands, their subsequent activation, and the interplay between innate and adaptive immunity are considered pivotal in driving disease development and progression [5]. Understanding these mechanisms requires robust experimental models that recapitulate the multifaceted features of human disease while allowing controlled investigation of temporal dynamics and mechanistic pathways.

Animal models have been instrumental in advancing our understanding of SjD pathogenesis and evaluating potential therapeutic interventions. Various genetic and induced animal models have been developed, each offering distinct advantages for studying specific aspects of the disease. Among spontaneous models, the non-obese diabetic (NOD) mouse represents a prototypical genetically predisposed strain that develops both type 1 diabetes and SjD-like autoimmune exocrinopathy. NOD mice spontaneously develop lymphocytic infiltration in salivary and lacrimal glands between 8 and 16 weeks of age, with detectable serum autoantibodies and progressive decline in salivary flow rates after 16 weeks [6,7]. Congenic strains derived from the NOD background, such as NOD-*Aec1/2* (C57BL/6.NOD-*Aec1Aec2*), carry specific genetic intervals that accelerate disease onset and severity, providing refined tools for mechanistic studies [8–10]. Induced models, generated through exogenous stimuli such as viral infection or immunization with glandular extracts or SjD-associated autoantigens, offer complementary approaches for investigating early pathogenic events [11]. However, these conventional murine models, while valuable, possess inherent limitations in translating findings to human disease due to fundamental differences in immune system components, particularly major histocompatibility complex (MHC) molecules.

To bridge the translational gap between murine models and human disease, there has been growing interest in developing humanized animal models that incorporate human cellular or genetic elements. The first humanized SjD model was established by Young et al., who transferred freshly isolated peripheral blood mononuclear cells (PBMCs) from SjD patients into immunodeficient NOD-*scid* gamma (NSG) mice, demonstrating that human immune cells could reconstitute and drive glandular pathology [12]. Subsequent refinements have enhanced this approach, including combinations with salivary gland protein immunization to induce more robust disease phenotypes [13,14]. While these PBMC-transfer models provide valuable platforms for studying patient-derived immune responses, they represent transient systems with inherent limitations in modeling chronic disease progression and lack the genetic stability required for long-term mechanistic studies. An alternative and complementary approach to humanization involves incorporating human genetic elements directly into the host genome, particularly human leukocyte antigen (HLA) molecules that govern antigen presentation and T-cell recognition. Among HLA class II alleles, HLA-DR3 (specifically HLA-DRB1*03:01) has emerged as a

prominent genetic risk factor for SjD across multiple populations [15,16]. Given the strong genetic association between HLA-DR3 and human SjD, incorporating this risk allele into an established autoimmune-prone genetic background represents a rational strategy for developing a more translationally relevant model. The NOD-DR3 mouse strain represents this approach: NOD-congenic mice in which endogenous mouse MHC class II molecules have been eliminated and replaced with human HLA-DR3 molecules via the DR3(DRw17) transgene, which expresses the HLA-DRA0101 and HLA-DRB10301 alleles [17]. This model has been successfully utilized to study various experimental autoimmune diseases [18,19]; however, it has never been systematically characterized for SjD-related phenotypes.

The present study was undertaken to comprehensively characterize the NOD-DR3 mouse strain as a novel humanized model for SjD. We hypothesized that replacement of mouse MHC class II with human HLA-DR3 molecules in the autoimmune-prone NOD background would recapitulate the cardinal features of human SjD, including salivary gland secretory dysfunction, production of disease-specific autoantibodies, and lymphocytic infiltration of exocrine glands. Furthermore, given the pronounced female bias in human SjD and the known influences of sex hormones on immune responses, we specifically investigated whether NOD-DR3 mice exhibit sex dimorphism in disease manifestations. Our findings demonstrate that NOD-DR3 mice reproduce the clinical, serological, histological, and immunological hallmarks of SjD with remarkable fidelity to human disease. The model exhibits sex dimorphism across all measured parameters, providing unique opportunities to dissect the mechanistic basis of sex bias in autoimmunity. The availability of this genetically stable, humanized model represents a significant advancement in translational SjD research, offering a critical bridge between conventional murine systems and human clinical disease.

2. Materials and Methods

2.1. Mice

NOD-DR3 mice were obtained from the lab of Dr. Yaron Tomer, Albert Einstein College of Medicine, New York. Mice were allowed to acclimate to the facility for at least two weeks before handling. The other mice used here were as follows: C57BL/6 J.NOD-*Aec1Aec2* (NOD-*Aec1/2*) and control mice C57BL/6 J (B6), and NOD/ShiLtJ (NOD). All mice were housed under specific pathogen-free conditions in the animal facilities of the University of Florida Animal Care Services. All the procedures related to the use of animals were approved by the University of Florida Institutional Animal Care and Use Committee (IACUC) under the approved protocol (IACUC202300000418). All methods were performed in accordance with the relevant guidelines and regulations. All animals were maintained on a 12 h light–dark schedule, and food and acidified water were provided ad libitum. At times indicated in the study, mice were euthanized, after deep anesthetization with isoflurane, by cervical dislocation, and their organs and tissues were freshly harvested for analyses.

2.2. Measurement of Saliva Flow Rates

To measure stimulated saliva flow rates, individual mice were weighed and given an intraperitoneal (ip) injection of 100 µL of a mixture containing isoproterenol (0.2 mg/1 mL) and pilocarpine (0.05 mg/1 mL) in PBS. Saliva was collected for 10 min from the oral cavity of individual mice using a micropipette starting one minute after injection of isoproterenol and pilocarpine; the volume of each saliva sample was measured.

2.3. Histological Examination of the Salivary and Lacrimal Glands

Salivary (submandibular, sublingual, and parotid) and lacrimal glands, excluding cervical draining lymph nodes, were explanted and fixed in 10% phosphate-buffered formalin for 48 h. Fixed tissues were embedded in paraffin and sectioned at a thickness of 5 µm. The prepared tissue sections were stained with hematoxylin and eosin (H&E) dye. Slides were scanned using the Aperio GT 450 at ×400 magnification mode (Leica Biosystems, Deer Park, IL, USA). To detect and determine leukocytic infiltrations in salivary glands, a single histological section per gland per mouse was examined by a blinded examiner. Lymphocytic infiltrations were defined as aggregates of >50 leukocytes/4 mm^2.

2.4. Evaluation of Antinuclear Antibody Staining Patterns

Examination of antinuclear antibody staining patterns was performed as previously described. In brief, sera were diluted 1:40 in PBS and incubated on permeabilized HEp2 ANA slides (ImmunoConcepts, Sacramento, CA, USA) prior to incubation with FITC secondary antibody. Sections were observed at 200× magnification using a Nikon Eclipse Ti-E inverted microscope (Nikon USA, Melville, NY, USA).

2.5. Determination of SjD-Associated Autoantibodies

96-well plates were coated with recombinant mouse antigen Ro52/SS-A, Ro60/SS-A, and La/SS-B (Surmodics, Eden Prairie, MN, USA) (0.6 ug/mL in carbonate buffer pH 9.6, overnight, 4 °C). The plate was blocked with 5% bovine serum albumin (1 h, 4 °C). A total of 200 uL of a 1:20 dilution of sera was added into each well in triplicate. Sera from mice were incubated at room temperature for 2 h. The plate was then washed with PBS-T, treated with a 1:10,000 dilution of anti-mouse IgG (#SC-2005, Santa Cruz Biotech, Santa Cruz, CA, USA) conjugated to horseradish peroxidase (HRP) in PBS, and incubated for 2 h at room temperature. After washing the plate with PBS-T, the wells were treated with 100 uL of TMB substrate solution (#00-4201-56, eBioscience, San Diego, CA, USA) for 30 m with shaking, then with 3N HCl to stop the reaction. The plate was read at an absorbance of 450 nm using a Tecan Infinite M200 Pro spectrophotometric plate reader (Tecan, Mannedorf, Switzerland). The data was recorded as relative absorbance.

2.6. Examination of Salivary Gland Infiltrating Lymphocytes

Single-cell suspensions were prepared from salivary glands as previously described [20]. Briefly, salivary glands were placed in RPMI (Gibco, Waltham, MA, USA) complete media in a MACS C tube (Miltenyi Biotec, San Diego, CA, USA) for desiccation on GentleMACS V1.02 (38 s, twice). After a 10 min incubation at 37 °C the media was removed into cold RPMI complete media and held at 4 °C. Warm media was replenished and the process was repeated twice more. Single-cell suspensions were centrifuged (2500 rpm, 10 min, 4 °C) and resuspended in PBS for filtration through a 70-µm sterile cell strainer (Fisher, Pittsburgh, PA, USA). After a wash with PBS, cells were resuspended again in PBS for lymphocyte isolation with Lympholyte–M cell separation media (Cedar Lane, Bulington, ON, Canada) per manufacturer's instructions. Ex vivo single-cell suspensions were washed with PBS, then stained with TruStain FcX (Biolegend, San Diego, CA, USA) before staining for the following markers: T-cell profile: PE-Cy5 anti-mouse CD3 (Biolegend, San Diego, CA, USA, 145-2C11), BV605 anti-mouse CD4 (Biolegend, GK1.5), BV570 anti-mouse CD8 (Biolegend, 53-6.7), PE anti-mouse gamma/delta (Biolegend, GL3), APC-Cy7 anti-mouse Nkp46 (Biolegend, 29A1.4), BV785 anti-mouse CD68 (Biolegend, FA-11). Intracellular staining was done using IL-4 PE-Cy7 (Biolegend, 11B11), BV421 anti-mouse IL-9 (Biolegend, RM9A4), AF488 anti-mouse IL-17 (BD Biosciences, Franklin Lakes, NJ, USA, TC11-18H10), APC for IFN-Gamma (Biolegend, XMG1.2), and PerCP-eF710 anti-mouse

RORgT (eBioscience, B2D); B-cell profile: Pacific blue anti-mouse CD1 (Biolegend, 1B1), AF647 anti-mouse CD5 (BD Biosciences, 53-7.3), PE-Cy5 (Biolegend, 6D5), PE Cy7 anti-mouse CD21 (Biolegend, 7E9), FITC anti-mouse CD23 (Biolegend, B3B4) BV785 anti-mouse B220 (Biolegend, RA3-6B2), BV605 anti-mouse CD138 (Biolegend, 281-2), PE Fas (Biolegend, SA367H8), PerCP-Cy5.5 anti-mouse GL7 (Biolegend, GL7), AF700 anti-mouse (Biolegend, 11-26c.2a), APC-Cy7 anti-mouse IgM (Biolegend, RMM-1) with AmCyan as a live dead marker (ThermoFisher Waltham, MA, USA) for both. The samples were analyzed using Cytek Full Spectrum Viewer (Cytek Biosciences, Fremont, CA, USA) with a gating strategy as previously described [21], and the analysis was performed using FlowJo, v10.10.2 software (FlowJo, Ashland, OR, USA).

2.7. Statistics

Statistical analyses were performed using Prism 11.0.0 version (GraphPad Software, Boston, MA, USA). Where indicated, statistical comparisons were performed using one-way ANOVA, two-way ANOVA, and the chi-square test. In all cases, *p*-values less than 0.05 were considered significant.

3. Results

3.1. NOD-DR3 Showed the Loss of Salivary Gland Secretory Function

NOD-DR3 are NOD-congenic mice in which the endogenous mouse MHC class II has been eliminated and replaced with human HLA class II molecules via the DR3(DRw17) transgene. This transgene expresses the HLA-DR3 genotype (HLA-DRA0101 and HLA-DRB10301). While the model has been utilized to study several experimental autoimmune diseases, it has not been previously characterized for SjD phenotypes. We therefore investigated whether NOD-DR3 mice recapitulate the cardinal clinical features of SjD, including salivary gland secretory dysfunction, autoantibodies, and glandular lymphocytic infiltrations. Based on our previous observations that mouse models of SjD typically demonstrate initial loss of salivary secretory function around 20–24 weeks of age, we assessed whether NOD-DR3 mice exhibit a similar temporal pattern. Saliva was collected from mice aged 20–32 weeks and analyzed alongside two established SjD models (NOD-*Aec1/2* and NOD) and a healthy B6 control. As shown in Figure 1A, NOD-DR3 mice displayed significantly reduced salivary flow rates (SFRs; 5.33 $\pm$ 0.45 µL/min) that were comparable to both NOD-*Aec1/2* (5.36 $\pm$ 0.37 µL/min) and NOD (4.27 $\pm$ 0.24 µL/min) mice, representing an approximately 54% reduction compared to B6 control mice (11.65 $\pm$ 0.51 µL/min). To determine whether NOD-DR3 mice exhibit sex-based differences in salivary dysfunction, we analyzed SFR separately in male and female cohorts. As shown in Figure 1B, both sexes showed a similar reduction in SFR, comparable to that observed in established SjD models, indicating the absence of significant sex dimorphism in this phenotype. These findings demonstrate that NOD-DR3 mice develop salivary gland secretory dysfunction characteristic of SjD, with severity and kinetics comparable to validated SjD mouse models.

3.2. NOD-DR3 Mice Express SjD-Associated Autoantibodies with Sex-Dependent Patterns

Autoantibodies represent the hallmark serological feature of Sjögren's disease (SjD); therefore, we investigated whether NOD-DR3 mice produce SjD-associated autoantibodies. Analysis of antinuclear antibody (ANA) prevalence revealed that 70% of NOD-DR3 mice were ANA-positive, comparable to the two established SjD models (Figure 2A). To assess potential sex dimorphism in autoantibody production, we analyzed male and female cohorts separately. Male NOD-DR3 mice exhibited a higher ANA frequency than females (77% vs. 57%), mirroring the sex-based pattern observed in the NOD model (Figure 2B). Further characterization of ANA staining patterns, which reflect distinct autoantibody

specificities, revealed notable sex differences. Male NOD-DR3 mice displayed predominantly homogeneous and nucleolar staining patterns, whereas females showed primarily speckled patterns (Figure 2C). Notably, the nucleolar pattern was unique to male NOD-DR3 mice and absent in both sexes of the other SjD models, while the speckled pattern was present in females across all three SjD models but reduced in male NOD-DR3 mice.

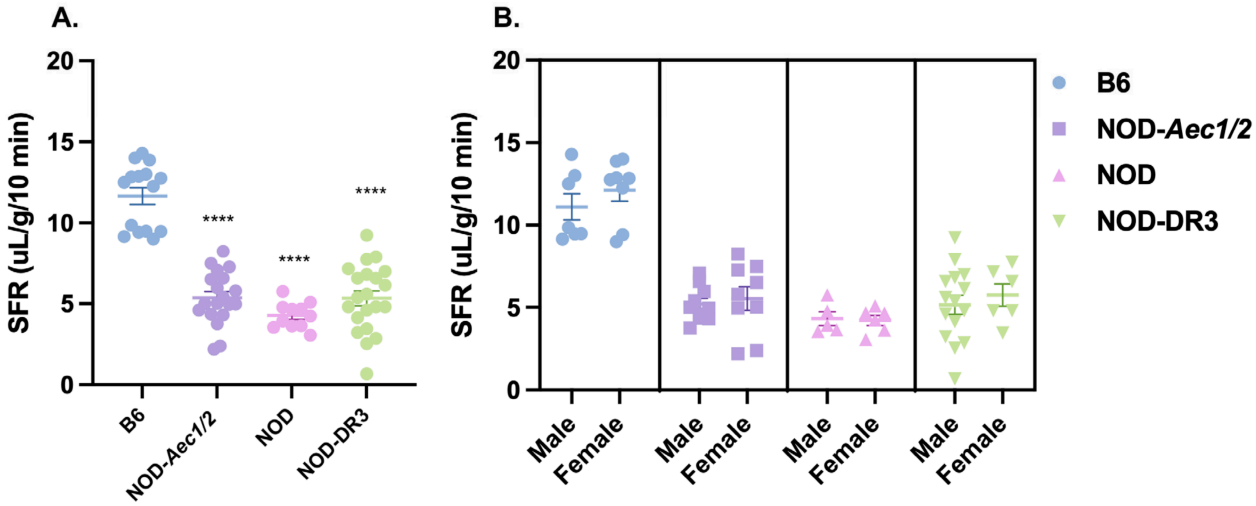


Figure 1. NOD-DR3 mice exhibit reduced salivary flow rates, comparable to those in established SjD animal models. Saliva was collected from mice aged 20–32 weeks following pilocarpine/isoproterenol stimulation. (**A**) Salivary flow rates (SFRs, µL/min) in NOD-DR3 (n = 21) mice compared to two established SjD models (NOD-*Aec1/2*, n = 19, and NOD, n = 11) and healthy B6 control mice (n = 15). B6 vs. NOD-*Aec1/2*, 95% CI (4.81 to 7.76), $p < 0.0001$. B6 vs. NOD, 95% CI (5.69 to 9.08), $p < 0.0001$. B6 vs. NOD-DR3, 95% CI (4.88 to 7.76), $p < 0.0001$. (**B**) Sex-stratified analysis of salivary flow rates in male and female cohorts across all four mouse strains (B6, n = 8F, n = 7M; NOD-*Aec1/2*, n = 9F, n = 10M; NOD, n = 6F, n = 5M; NOD-DR3, n = 6F, n = 15M). Data are presented as mean ± SEM. Each symbol represents an individual mouse. Statistical significance was determined by one-way ANOVA. **** < 0.0001.

To further characterize the autoantibody profile, we quantified antibodies against specific SjD-associated autoantigens (Ro52, Ro60, and La) by ELISA. NOD-DR3 mice showed elevated anti-Ro52 levels compared to B6 controls, levels similar to those of NOD mice but lower than those of NOD-*Aec1/2* mice (Figure 3A). Comparable trends were observed for anti-Ro60 and anti-La antibodies (Figure 3B,C). Sex-stratified analysis revealed that female NOD-DR3 mice produced significantly higher levels of all three autoantibodies than males (Figure 3D,F). This female-predominant pattern paralleled that of NOD-*Aec1/2* mice, whereas NOD mice exhibited the opposite trend, with males showing higher autoantibody levels than females. Collectively, these findings demonstrate that NOD-DR3 mice develop robust autoantibody responses, including ANA and antibodies against Ro52, Ro60, and La autoantigens. Importantly, the model exhibits pronounced sex dimorphism in autoantibody profiles, recapitulating key serological features observed in established SjD mouse models.

3.3. NOD-DR3 Mice Exhibit Lymphocytic Infiltration in the Salivary and Lacrimal Glands

To determine whether NOD-DR3 mice recapitulate the glandular pathology observed in SjD patients, we quantified focus scores (FS) in the salivary and lacrimal glands (Supplementary Figure S1). NOD-DR3 mice exhibited significantly elevated FS compared to B6 controls in both gland types (Figure 4A,B). To further characterize these differences, we stratified the analysis by sex. In the salivary glands, female NOD-DR3 mice displayed higher FS than their male counterparts, a pattern also observed in NOD mice (Figure 4C).

Notably, this sex-specific trend was reversed in the lacrimal glands, where male NOD-DR3 mice exhibited higher FS than females (Figure 4D), suggesting a gland-specific influence of sex on focal lymphocytic infiltration.

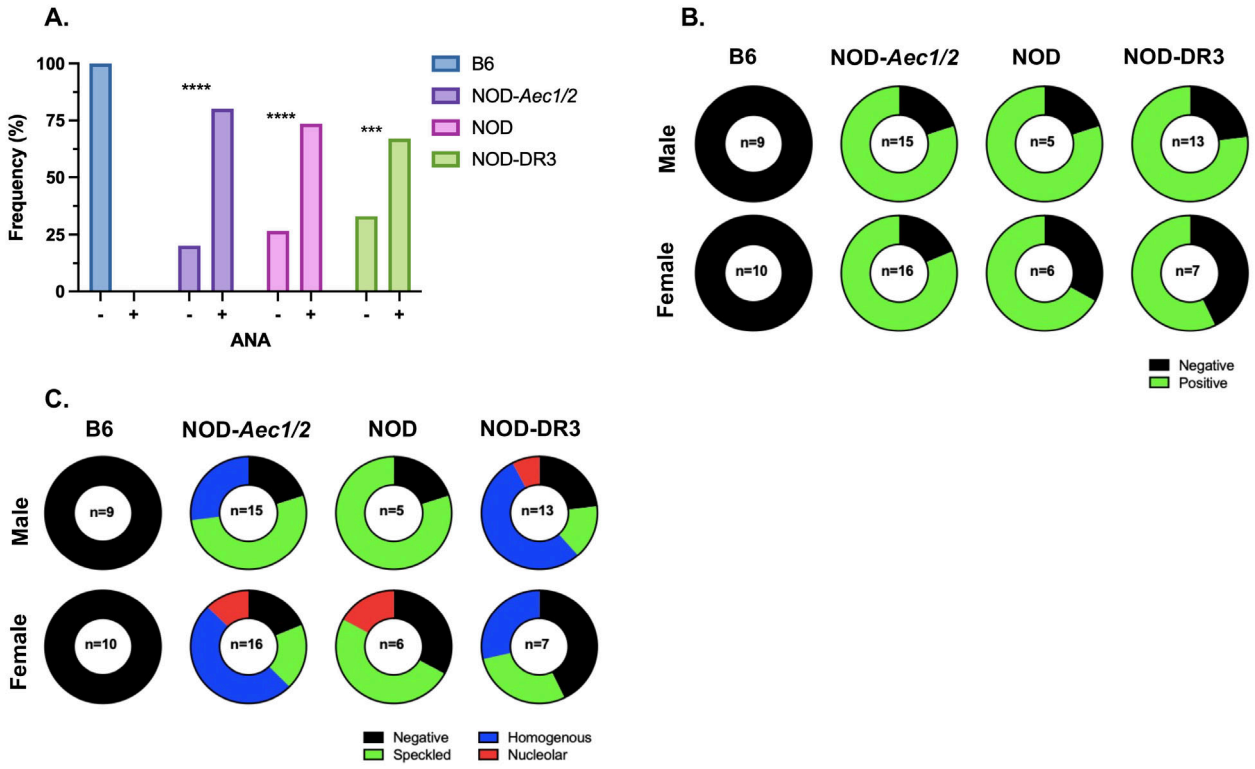


Figure 2. NOD-DR3 mice express antinuclear antibodies with sex-dependent patterns. Serum samples from aged mice (20–32 weeks) were analyzed for ANA prevalence and staining patterns. (**A**) Percentage of ANA-positive and ANA-negative mice across B6, NOD-*Aec1/2*, NOD, and NOD-DR3 strains. Seventy percent of NOD-DR3 mice were ANA-positive, comparable to the two established SjD models. (**B**) Sex-stratified analysis of ANA prevalence. Male NOD-DR3 mice exhibited higher ANA frequency than females (77% vs. 57%) with no statistical significance ($p = 0.34$), mirroring the pattern observed in NOD mice. (**C**) ANA staining pattern analysis by immunofluorescence. Male NOD-DR3 mice displayed predominantly homogeneous and nucleolar patterns, while females showed primarily speckled patterns. Data are presented as percentages or frequency distributions. Statistical comparisons were performed using the chi-square test with a two-tailed *p*-value. *** $p < 0.001$, and **** $p < 0.0001$.

To better define the cellular composition of glandular infiltrates, we isolated single cells from the salivary glands and performed a comprehensive flow cytometric analysis of B- and T-cell populations in a sex-dependent manner. Analysis of total B-cell infiltration revealed striking sex dimorphism in NOD-DR3 mice, with females expressing a significantly higher percentage of B-cells compared to males (5.79 ± 1.61% vs. 0.46 ± 0.06%), representing an approximately 12-fold difference. This female-predominant pattern was consistently observed across the established SjD models (NOD-*Aec1/2* and NOD), while the healthy B6 control strain showed no appreciable sex-based differences, indicating that this is a disease-associated phenomenon rather than a general biological difference between sexes. Further dissection of B-cell subsets provided additional insight into the nature of the humoral immune response. When we analyzed follicular B cell subsets (FO I and FO II) and germinal center (GC) B cells, populations critical for antibody production and affinity maturation, female NOD-DR3 mice consistently showed higher percentages of these populations than males (Figure 5), with absolute cell counts presented (Supplementary Table S1).

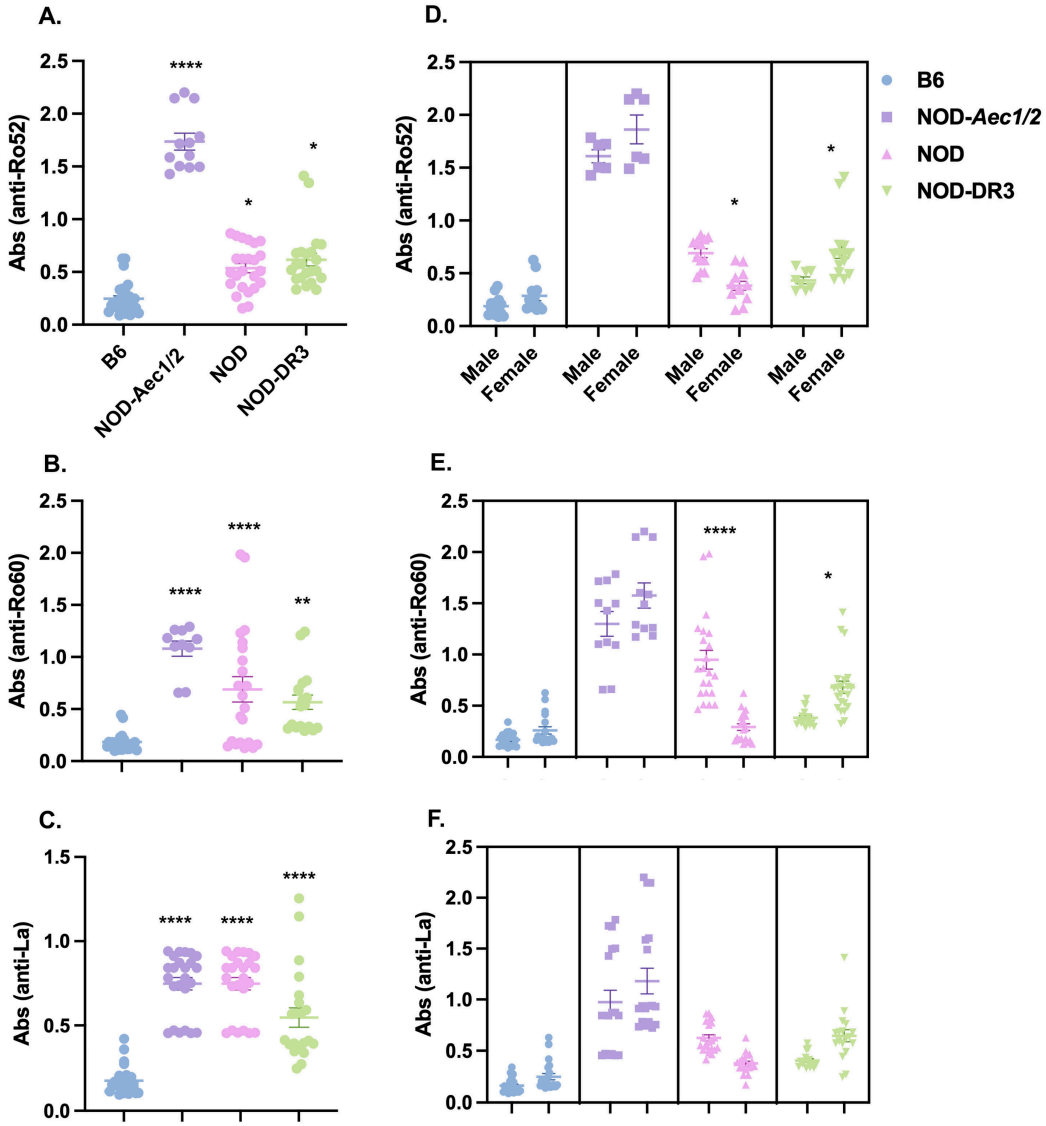


Figure 3. NOD-DR3 mice produce elevated levels of anti-Ro and anti-La autoantibodies with pronounced sex dimorphism. Serum levels of autoantibodies against SjD-associated autoantigens were quantified by ELISA. (**A**) Anti-Ro52 (B6, $n = 28$; NOD-*Aec1/2*, $n = 12$; NOD, $n = 24$; NOD-DR3, $n = 22$), B6 vs. NOD-*Aec1/2*, 95% CI (−1.72 to −1.26), $p < 0.0001$. B6 vs. NOD, 95% CI (−0.42 to −0.16), $p < 0.0001$. B6 vs. NOD-DR3, 95% CI (−0.54 to −0.20), $p < 0.0001$; (**B**) anti-Ro60 (B6, $n = 22$; NOD-*Aec1/2*, $n = 10$; NOD, $n = 22$; NOD-DR3, $n = 18$, B6 vs. NOD-*Aec1/2*, 95% CI (−1.23 to −0.56), $p < 0.0001$. B6 vs. NOD, 95% CI (−0.77 to −0.24), $p < 0.0001$. B6 vs. NOD-DR3, 95% CI (−0.66 to −0.10), $p = 0.0043$; (**C**) anti-La (B6, $n = 26$; NOD-*Aec1/2*, $n = 24$; NOD, $n = 24$; NOD-DR3, $n = 22$), B6 vs. NOD-*Aec1/2*, 95% CI (−0.70 to −0.45), $p < 0.0001$. B6 vs. NOD, 95% CI (−0.67 to −0.45), $p < 0.0001$. B6 vs. NOD-DR3, 95% CI (−0.50 to −0.24), $p < 0.0001$. NOD-DR3 mice showed elevated levels of all three autoantibodies compared to B6 controls, with levels similar to NOD mice but lower than NOD-*Aec1/2* mice. Sex-stratified analysis of (**D**) anti-Ro52 (B6, $n = 12$F, $n = 14$M; NOD-*Aec1/2*, $n = 6$F, $n = 6$M; NOD, $n = 12$F, $n = 12$M; NOD-DR3, $n = 14$F, $n = 8$M), NODF vs. M, 95% CI (−0.60 to −0.09), $p = 0.02$, NOD-DR3F vs. M, 95% CI (−0.55 to −0.03), $p = 0.02$ (**E**) anti-Ro60 (B6, $n = 18$F, $n = 20$M; NOD-*Aec1/2*, $n = 11$F, $n = 11$M; NOD, $n = 20$F, $n = 22$M; NOD-DR3, $n = 22$F, $n = 16$M), NODF vs. M, 95% CI (0.40 to 0.92), $p < 0.0001$, NOD-DR3F vs. M, 95% CI (−0.57 to −0.02), $p = 0.02$ and (**F**) anti-La (B6, $n = 21$F, $n = 22$M; NOD-*Aec1/2*, $n = 20$F, $n = 20$M; NOD, $n = 20$F, $n = 22$M; NOD-DR3, $n = 18$F, $n = 16$M). Female NOD-DR3 mice produced significantly higher levels of all three autoantibodies compared to males. Data are presented as mean ± SEM with each symbol representing an individual mouse. Statistical comparisons were performed using one-way ANOVA with Tukey's multiple comparisons test. * $p < 0.05$, ** $p < 0.01$, and **** $p < 0.0001$.

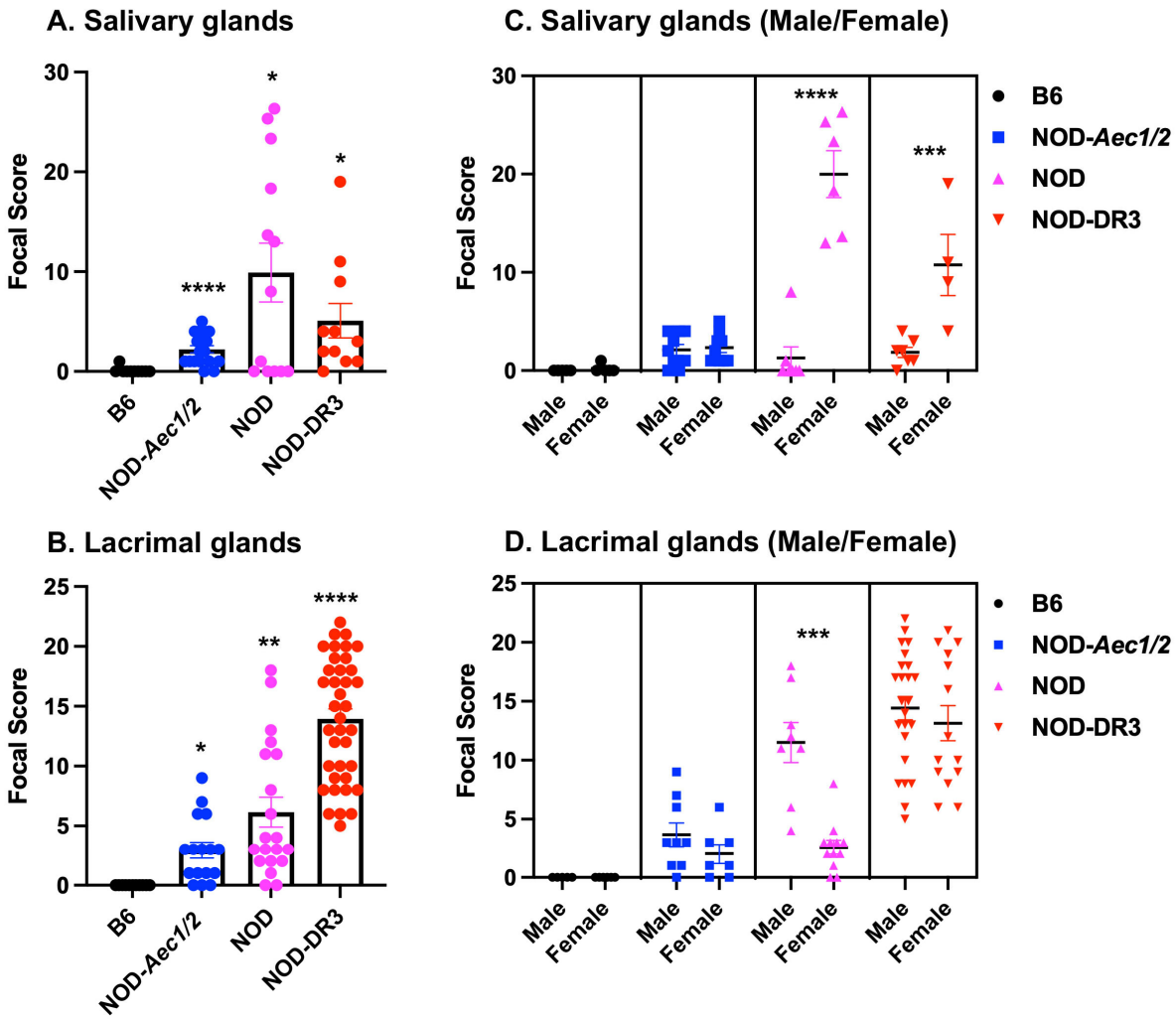


Figure 4. NOD-DR3 mice develop lymphocytic infiltration of the salivary and lacrimal glands, with greater severity in females in the salivary glands. Whole salivary and lacrimal glands from aged mice (20–32 weeks) were processed for histological analysis. Focal scores, representing the number of lymphocytic foci (≥50 lymphocytes) per 4 mm^2 of glandular tissue, were quantified. (**A**) Focal scores in salivary glands across mouse strains. NOD-DR3 salivary glands showed moderate infiltration (5.09 ± 1.73), intermediate between NOD-*Aec1/2* (2.22 ± 0.37) and NOD (9.92 ± 2.95), while B6 controls showed no detectable infiltration. (B6, n = 10; NOD-*Aec1/2*, n = 18; NOD, n = 13; NOD-DR3, n = 11). B6 vs. NOD-*Aec1/2* (95% CI (−3.11 to −1.13), $p < 0.0001$), B6 vs. NOD, 95% CI (−17.93 to −1.72), $p = 0.0173$. B6 vs. NOD-DR3, 95% CI (−9.89 to −0.09), $p = 0.046$. (**B**) Focal scores in lacrimal glands. NOD-DR3 exhibited the most severe lacrimal gland infiltration (13.95 ± 0.83), substantially higher than both NOD-*Aec1/2* (2.94 ± 0.68) and NOD (6.25 ± 1.25). (B6, n = 11; NOD-*Aec1/2*, n = 16; NOD, n = 20; NOD-DR3, n = 38). B6 vs. NOD-*Aec1/2* (95% CI (−7.13 to 1.25), $p = 0.049$. B6 vs. NOD, 95% CI (−10.16 to −2.14), $p = 0.0015$. B6 vs. NOD-DR3, 95% CI (−17.61 to −10.29), $p < 0.0001$. (**C**) Sex-stratified analysis of salivary gland focal scores. Female NOD-DR3 mice demonstrated significantly higher focal scores than males (10.75 ± 3.12 vs. 1.86 ± 0.51), paralleling the NOD model (Female: 20.00 ± 2.39 vs. Male: 1.29 ± 1.13). (B6, n = 5, n = 5M; NOD-*Aec1/2*, n = 9F, n = 9M; NOD, n = 6F, n = 7M; NOD-DR3, n = 4F, n = 7M). NODF vs. M, 95% CI (−24.01 to −13.42), $p < 0.0001$, NOD-DR3F vs. M, 95% CI (−14.86 to −2.92), $p = 0006$. (**D**) Sex-stratified analysis of lacrimal gland focal scores (B6, n = 6F, n = 5M; NOD-*Aec1/2*, n = 7F, n = 9M; NOD, n = 12F, n = 8M; NOD-DR3, n = 14F, n = 24M). NODF vs. M, 95% CI (3.14 to 14.69), $p = 0.0002$. Male NOD-DR3 mice exhibited higher focal scores than females, a male-predominant pattern consistently observed across all three SjD models. Data are presented as mean ± SEM. Each symbol represents an individual mouse. Statistical comparisons were performed using one-way ANOVA with Tukey's multiple comparisons test. * $p < 0.05$, ** $p < 0.01$, *** $p < 0.001$, and **** $p < 0.0001$.

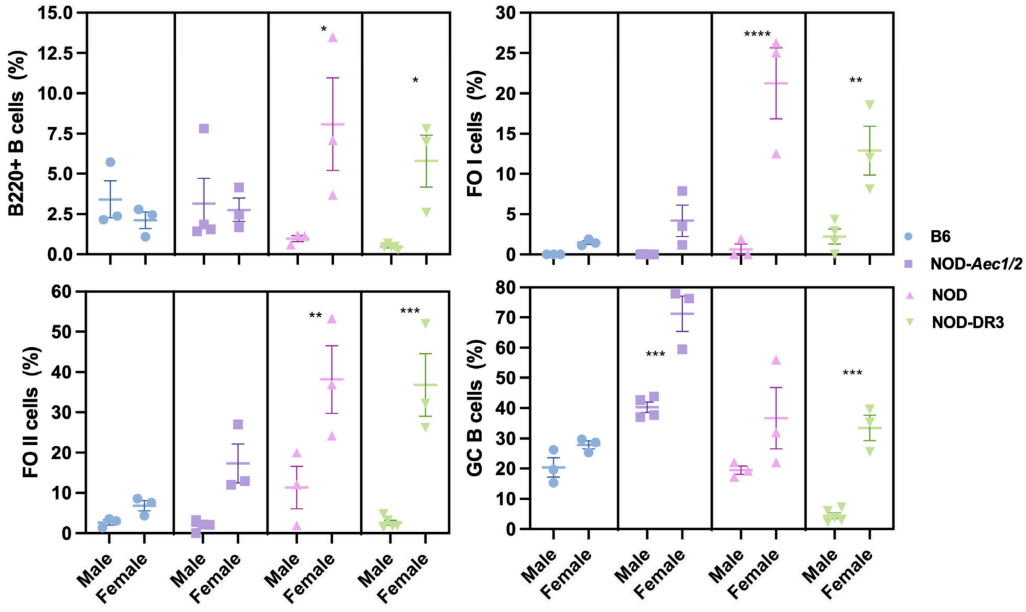


Figure 5. Female NOD-DR3 mice exhibit enhanced B-cell infiltration in salivary glands. Single-cell suspensions from salivary glands of aged mice (20–32 weeks) were analyzed by flow cytometry for B-cell populations. Bar graphs show percentages of B-cell subsets in male and female cohorts across B6, NOD-*Aec1/2*, NOD, and NOD-DR3 strains. (B6, n = 3F, n = 3M; NOD-*Aec1/2*, n = 3F, n = 4M; NOD, n = 3F, n = 3M; NOD-DR3, n = 3F, n = 5M). Female NOD-DR3 mice expressed significantly higher percentages of total B cells. This female-predominant pattern was consistently observed for FO I, FO II, and GC B cells. B220+ B cells: NODM vs. F, 95% CI (−13.83 to −0.39), p = 0.0345. NOD-DR3M vs. F, 95% CI (−12.62 to 0.40), p = 0.05. FO I: NODM vs. F, 95% CI (−29.78 to −11.48), p < 0.0001. NOD-DR3M vs. F, 95% CI (−19.24 to −2.11), p = 0.0088. FO II: NODM vs. F, 95% CI (−48.04 to −5.54), p = 0.0079. NOD-DR3M vs. F, 95% CI (−53.18 to −15.17), p = 0.0002. GC B cells: NOD-*Aec1*/2M vs. F, 95% CI (−50.23 to −11.62), p = 0.0007. NOD-DR3M vs. F, 95% CI (−47.48 to −10.57), p = 0.0008. Data are presented as mean ± SEM, with each bar representing the group average. Statistical comparisons were performed using one-way ANOVA with Tukey's multiple comparisons test. * p < 0.05, ** p < 0.01, *** p < 0.001, and **** p < 0.0001.

Analysis of T-cell populations revealed a more nuanced pattern of sex dimorphism than that observed in B-cells. Female NOD-DR3 mice demonstrated significantly higher percentages of several key lymphocyte populations, including CD4+ T-cells, CD8+ T cells, natural killer (NK) cells, and Th17 cells. The elevated Th17 population in females is particularly significant, as this subset produces IL-17 and other proinflammatory cytokines that promote tissue inflammation and have been implicated in autoimmune pathology. The higher CD4+ T cell frequency in females likely reflects enhanced T-cell help for B-cell responses, consistent with the elevated B-cell infiltration and autoantibody production observed in female mice. Interestingly, males exhibited a distinct immunological profile characterized by higher percentages of macrophages, Th1 cells, and Th9 cells, while Th2 cell percentages remained comparable between sexes (Figure 6), with absolute cell counts presented (Supplementary Table S1). Comparative analysis across the different mouse strains revealed that the sex-dependent immunological patterns in NOD-DR3 mice largely recapitulate those observed in established SjD models. In CD4+ T cells, NK cells, macrophages, Th1 cells, and Th17 cells, both male and female NOD-DR3 mice showed trends similar to those in NOD and NOD-*Aec1/2* strains, indicating that these sex-based differences represent conserved features of SjD pathogenesis rather than model-specific artifacts. This conservation across multiple genetic backgrounds strengthens the biological relevance of these findings and suggests that HLA-DR3-restricted immune responses maintain the fundamental sex dimorphism characteristic of murine SjD models. Collectively,

these cellular analyses demonstrate that NOD-DR3 mice exhibit profound sex dimorphism in salivary gland immune infiltration, with females showing enhanced B cell-mediated responses and specific T helper subsets, while males display elevated Th1-type immunity.

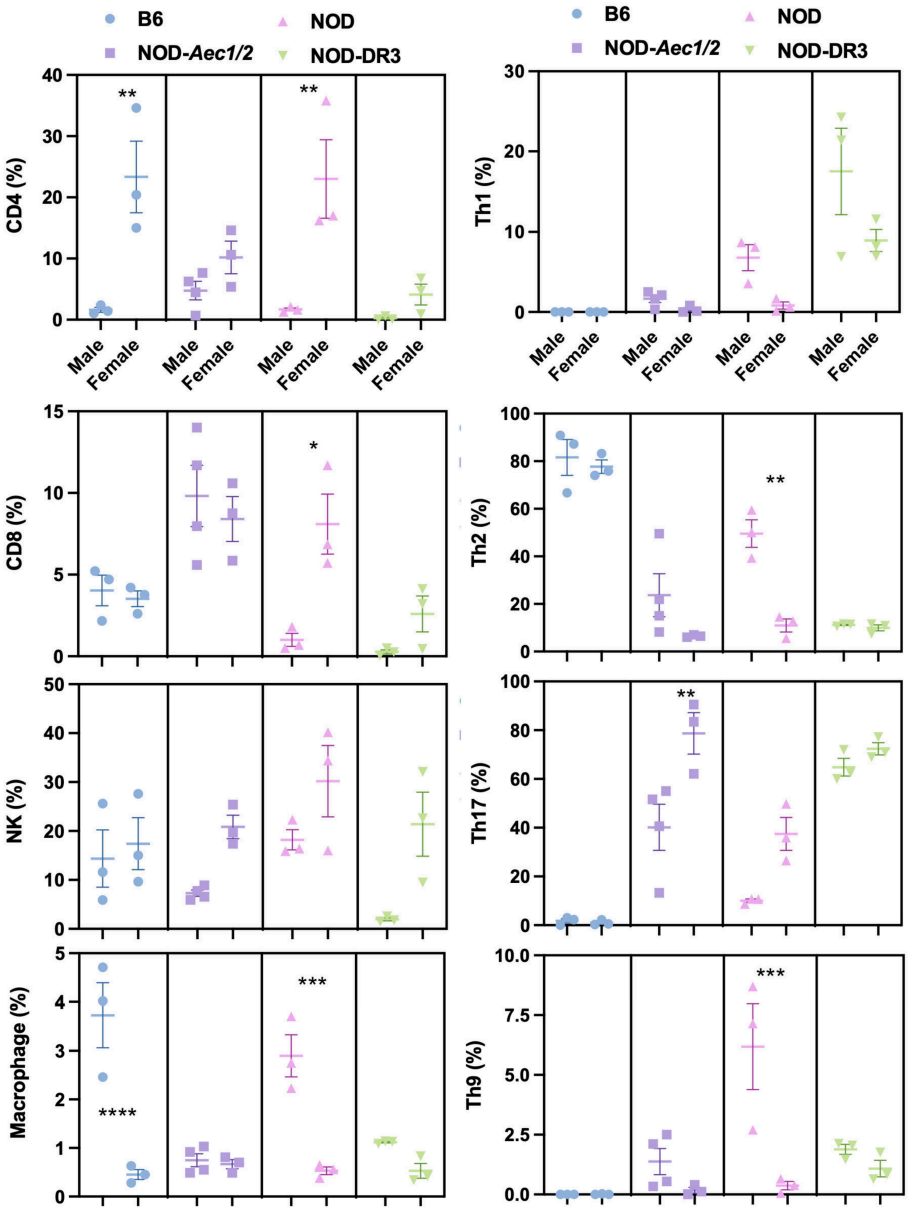


Figure 6. NOD-DR3 mice display specific sex-dependent immune cell patterns in salivary glands. Flow cytometric analysis of T cells and their subsets, NK, and macrophages in salivary gland single-cell suspensions from aged mice (20–32 weeks). Bar graphs display the percentages of T-cell subsets, NK cells, and macrophages in male and female cohorts across mouse strains. Female NOD-DR3 mice had higher percentages of CD4+ T cells, CD8+ T cells, NK cells, and Th17 cells than males. In contrast, males exhibited higher percentages of macrophages, Th1 cells, and Th9 cells, while Th2 cell percentages remained comparable between sexes. (B6, n = 3F, n = 3M; NOD-*Aec1/2*, n = 3F, n = 4M; NOD, n = 3F, n = 3M; NOD-DR3, n = 3F, n = 3M). CD4+ T cells: B6M vs. F, 95% CI (−37.52 to −5.90), p = 0.0039. NODM vs. F, 95% CI (−37.14 to −5.52), p = 0.0046. CD8+ T cells: NODM vs. F, 95% CI (−13.50 to −0.67), p = 0.0247. Macrophage: B6M vs. F, 95% CI (1.87 to 4.69), $p < 0.0001$. NODM vs. F, 95% CI (0.96 to 3.78), p = 0.0005. Th2: NODM vs. F, 95% CI (11.13 to 66.14), p = 0.0031. Th17: NOD. *Aec1*/2M vs. F 95% CI (−66.38 to −10.76), p = 0.0035. Th9: NODM vs. F, 95% CI (2.47 to 9.16), p = 0.0003. Data are presented as mean ± SEM. Each bar represents the group average across multiple mice. Statistical comparisons were performed using one-way ANOVA with Tukey's multiple comparisons test. * $p < 0.05$, ** $p < 0.01$, *** $p < 0.001$, and **** $p < 0.0001$.

4. Discussion

This study represents the first comprehensive characterization of NOD-DR3 mice as a model for SjD, demonstrating that these humanized HLA-DR3 transgenic mice recapitulate the cardinal clinical, serological, histological, and immunological features of the disease. Our findings reveal that NOD-DR3 mice exhibit significant salivary gland secretory dysfunction, robust production of disease-specific autoantibodies, including ANA and anti-Ro/La antibodies, and substantial lymphocytic infiltration in both the salivary and lacrimal glands. Notably, the model exhibits more severe lacrimal gland pathology than established SjD models, potentially offering greater translational relevance for studying ocular manifestations. A consistent and striking feature across all measured parameters was pronounced sex dimorphism, mirroring the female predominance observed in human SjD. Female mice demonstrated enhanced B-cell infiltration and humoral responses, while males exhibited distinct inflammatory profiles with elevated Th1. The humanized HLA-DR3 background provides a critical advantage for translational research, enabling investigation of HLA-restricted autoantigen presentation and immune responses directly relevant to human disease mechanisms. This comprehensive characterization establishes NOD-DR3 as a valuable addition to existing SjD models, offering unique opportunities to study disease pathogenesis and evaluate therapeutic interventions in a clinically relevant genetic context.

There are many unique animal models of SjD, including the spontaneous, transgenic, congenic, and induced models. Each model offers distinct advantages for studying specific aspects of SjD pathogenesis, from autoantibody production and cellular infiltration patterns to clinical manifestations. They offer temporal disease dynamics that are challenging to conduct in human patients. However, to enhance translational research, there is an impetus to incorporate human cellular or genetic elements to generate humanized animal models. The first humanized Sjögren's model was established by Young et al., who transferred freshly isolated human PBMCs from SjD patients into immunodeficient NOD-*scid* gamma (NSG) mice [12]. A refined approach was adopted by transferring PBMCs into NSG mice and combining this with subcutaneous immunization with salivary gland proteins from B6 mice, resulting in disease phenotypes characterized by upregulation of interferon-related genes [14]. A recent study using pre-activated PBMCs, and this pre-activation strategy specifically targets the CXCL9/10-CXCR3 axis, thereby maximizing CXCR3+ Th17 cell infiltration into salivary glands and recapitulating pathology within a 5-week window [13]. The current study employed a different approach: we profiled the NOD-congenic mouse model, in which endogenous mouse MHC class II molecules have been eliminated and replaced with the human HLA-DR3 transgene. The DR3 allele is one of the predominant alleles associated with SjD. DR3 haplotype patients in Latin America were shown to have more severe histopathology and to have anti-Ro and anti-La antibodies [22]. A similar association was identified, with strong linkage equilibrium, among Norwegian patients with primary SjD [23]. Interestingly, a study found that patients with a specific TCR repertoire and the HLA-DRA0101 allele produced more anti-Ro antibodies, suggesting antigen specificity in HLA-DR3 recognition [24]. Lastly, our previous study using in silico modeling has shown that HLA-DR3 has a high affinity for the core peptides of SjD-associated autoantigens (Ro52, Ro60, La), and, more importantly, we found that HLA-DR3 was predicted to bind with high affinity to specific viral and bacterial proteins [25]. Therefore, replacing the susceptible HLA alleles in an SjD-prone model recapitulates the SjD signature disease phenotypes.

One aspect of the study that remains intriguing is the dichotomy in the glandular B and T cells between males and females. Female NOD-DR3 exhibited higher B-cell infiltration, along with elevated levels of follicular and germinal center B-cells. This enhanced B-cell

response in females correlates directly with their higher autoantibody levels and more severe salivary gland pathology. T-cell analysis revealed complementary sex-dependent patterns. Females showed higher percentages of CD4+ T cells, CD8+ T cells, NK cells, and Th17 cells, while males exhibited elevated levels of macrophages, Th1 cells, and Th9 cells. The female-predominant Th17 response and male-predominant Th1/macrophage profile suggest distinct inflammatory pathways may contribute to sex-specific disease manifestations. As discussed, the peptide repertoire, which allows HLA-DR3 molecules to have specific binding grooves that preferentially present certain self-antigens, may favor those that drive T-cell responses, such as Th17 cells. Affinity and stability, which govern the strength and duration of HLA-DR3/peptide/TCR interactions, may also favor Th17 lineage commitment. Another critical factor that may skew the autoimmune response in males and females is the role of sex hormones. Estrogen, along with progesterone, regulates IL-17, Th17, and RORγt levels, a Th17-specific transcription factor [26,27]. Androgen can enhance macrophage migration and anti-inflammatory cytokine production, as we observed in the male mice [28]. In addition, the expansion of B cells, follicular and germinal center B cells, along with the increase in autoantibody response, could be attributed to the high level of estrogen in female NOD-DR3 mice, as estrogen is one of the main drivers for B cell proliferation, differentiation, and activation. It is directly involved in increasing antibody production [29].

Several limitations warrant consideration. The cross-sectional design at 20–32 weeks provides limited insight into disease progression and whether NOD-DR3 mice exhibit progressive pathology or early disease onset. Functional studies examining the mechanistic relationship between HLA-DR3-restricted antigen presentation and the observed phenotypes are needed to fully understand the autoantigenic peptide repertoire of DR3. Additionally, whether the unique nucleolar ANA pattern in male NOD-DR3 mice reflects clinically relevant autoantigen specificities requires further investigation. Overall, NOD-DR3 mice represent a valuable humanized model that replicates the clinical, serological, histological, and immunological features of SjD with pronounced and consistent sex dimorphism. The model's unique strengths—particularly severe lacrimal gland involvement and HLA-DR3-restricted immune responses—complement existing NOD-based models and offer enhanced translational potential for studying human disease mechanisms and testing therapeutic interventions targeting HLA-restricted pathways.

Supplementary Materials: The following supporting information can be downloaded at https://www.mdpi.com/article/10.3390/rheumato6040022/s1, Figure S1: Representative images of the salivary and lacrimal glands of the mice. Table S1: Flow cytometric analysis of the salivary glands.

Author Contributions: A.V. and S.G. performed the experiments presented in the study. A.V. and S.G. wrote the first draft of the manuscript. V.D. acquired and analyzed the histological images. D.L., P.G. and C.Q.N. conceptualized, analyzed, and participated in the preparation of the final manuscript. All authors have read and agreed to the published version of the manuscript.

Funding: This research was funded by the National Institute of Dental and Craniofacial Research grant number R56DE028544.

Institutional Review Board Statement: The animal study protocol was approved by the Institutional Animal Care and Use Committee of the University of Florida (protocol number IACUC202400000019 and approved on 9 September 2025).

Informed Consent Statement: Not applicable, no human subjects were used in the study.

Data Availability Statement: The original contributions presented in this study are included in the article/Supplementary Materials. Further inquiries can be directed to the corresponding author.

Acknowledgments: Research reported in this publication was supported by the National Institute of Dental & Craniofacial Research of the National Institutes of Health under Award Number R56DE028544. The content is solely the responsibility of the authors and does not necessarily represent the official views of the National Institutes of Health. We would like to thank Yaron Tomer at Albert Einstein College of Medicine for generously providing the NOD-DR3 mice.

Conflicts of Interest: The authors declare no conflicts of interest.

References

1. Witas, R.; Gupta, S.; Nguyen, C.Q. Contributions of Major Cell Populations to Sjögren's Syndrome. *J. Clin. Med.* **2020**, *9*, 3057. [CrossRef]
2. Nocturne, G.; Mariette, X. Sjogren Syndrome-Associated Lymphomas: An Update on Pathogenesis and Management. *Br. J. Haematol.* **2015**, *168*, 317–327. [CrossRef]
3. McCoy, S.S.; Hetzel, S.; VanWormer, J.J.; Bartels, C.M. Sex Hormones, Body Mass Index, and Related Comorbidities Associated with Developing Sjögren's Disease: A Nested Case-Control Study. *Clin. Rheumatol.* **2022**, *41*, 3065–3074. [CrossRef]
4. Tzioufas, A.G.; Wassmuth, R.; Dafni, U.G.; Guialis, A.; Haga, H.J.; Isenberg, D.A.; Jonsson, R.; Kalden, J.R.; Kiener, H.; Sakarellos, C.; et al. Clinical, Immunological, and Immunogenetic Aspects of Autoantibody Production against Ro/Ssa, La/Ssb and Their Linear Epitopes in Primary Sjogren's Syndrome (Pss): A European Multicentre Study. *Ann. Rheum. Dis.* **2002**, *61*, 398–404. [CrossRef]
5. Verstappen, G.M.; Corneth, O.B.J.; Bootsma, H.; Kroese, F.G.M. Th17 Cells in Primary Sjogren's Syndrome: Pathogenicity and Plasticity. *J. Autoimmun.* **2018**, *87*, 16–25. [CrossRef]
6. Robinson, C.P.; Yamachika, S.; Bounous, D.I.; Brayer, J.; Jonsson, R.; Holmdahl, R.; Peck, A.B.; Humphreys-Beher, M.G. A Novel Nod-Derived Murine Model of Primary Sjogren's Syndrome. *Arthritis Rheum.* **1998**, *41*, 150–156. [CrossRef]
7. van Blokland, S.C.; van Helden-Meeuwsen, C.G.; Wierenga-Wolf, A.F.; Drexhage, H.A.; Hooijkaas, H.; van de Merwe, J.P.; Versnel, M.A. Two Different Types of Sialoadenitis in the Nod- and Mrl/Lpr Mouse Models for Sjogren's Syndrome: A Differential Role for Dendritic Cells in the Initiation of Sialoadenitis? *Lab. Investig.* **2000**, *80*, 575–585. [CrossRef]
8. You, I.C.; Bian, F.; Volpe, E.A.; de Paiva, C.S.; Pflugfelder, S.C. Age-Related Conjunctival Disease in the C57bl/6.Nod-Aec1aec2 Mouse Model of Sjogren Syndrome Develops Independent of Lacrimal Dysfunction. *Investig. Ophthalmol. Vis. Sci.* **2015**, *56*, 2224–2233. [CrossRef]
9. Meng, W.; Li, Y.; Xue, E.; Satoh, M.; Peck, A.B.; Cohen, P.L.; Eisenberg, R.A.; Luning Prak, E.T. B-Cell Tolerance Defects in the B6.Aec1/2 Mouse Model of Sjogren's Syndrome. *J. Clin. Immunol.* **2012**, *32*, 551–564. [CrossRef]
10. Nguyen, C.; Singson, E.; Kim, J.Y.; Cornelius, J.G.; Attia, R.; Doyle, M.E.; Bulosan, M.; Cha, S.; Peck, A.B. Sjogren's Syndrome-Like Disease of C57bl/6.Nod-Aec1 Aec2 Mice: Gender Differences in Keratoconjunctivitis Sicca Defined by a Cross-over in the Chromosome 3 Aec1 Locus. *Scand. J. Immunol.* **2006**, *64*, 295–307. [CrossRef]
11. Chiorini, J.A.; Cihakova, D.; Ouellette, C.E.; Caturegli, P. Sjogren Syndrome: Advances in the Pathogenesis from Animal Models. *J. Autoimmun.* **2009**, *33*, 190–196. [CrossRef]
12. Young, N.A.; Wu, L.C.; Bruss, M.; Kaffenberger, B.H.; Hampton, J.; Bolon, B.; Jarjour, W.N. A Chimeric Human-Mouse Model of Sjögren's Syndrome. *Clin. Immunol.* **2015**, *156*, 1–8. [CrossRef]
13. Park, J.S.; Choi, J.; Jeong, H.Y.; Kang, H.Y.; Cho, S.H.; Lee, S.B.; Cho, M.L.; Park, S.H. Development of an Improved Preclinical Humanized Mouse Platform Representing the Diverse Clinical Phenotypes of Sjögren's Syndrome. *Front. Immunol.* **2026**, *17*, 1793493. [CrossRef]
14. Yang, Y.; Zhang, H.; Xiao, X.; Guo, M. Panoptosis Features, a Humanized Nsg Murine Model of Sjogren's Syndrome. *DNA Cell Biol.* **2024**, *43*, 207–218. [CrossRef]
15. Teos, L.Y.; Alevizos, I. Genetics of Sjogren's Syndrome. *Clin. Immunol.* **2017**, *182*, 41–47.
16. Reksten, T.R.; Lessard, C.J.; Sivils, K.L. Genetics in Sjogren Syndrome. *Rheum. Dis. Clin. N. Am.* **2016**, *42*, 435–447. [CrossRef]
17. Strauss, G.; Vignali, D.A.; Schönrich, G.; Hämmerling, G.J. Negative and Positive Selection by Hla-Dr3(Drw17) Molecules in Transgenic Mice. *Immunogenetics* **1994**, *40*, 104–108. [CrossRef]
18. Li, C.W.; Osman, R.; Menconi, F.; Concepcion, E.; Tomer, Y. Cepharanthine Blocks Tsh Receptor Peptide Presentation by Hla-Dr3: Therapeutic Implications to Graves' Disease. *J. Autoimmun.* **2020**, *108*, 102402. [CrossRef]
19. Li, C.W.; Menconi, F.; Osman, R.; Mezei, M.; Jacobson, E.M.; Concepcion, E.; David, C.S.; Kastrinsky, D.B.; Ohlmeyer, M.; Tomer, Y. Identifying a Small Molecule Blocking Antigen Presentation in Autoimmune Thyroiditis. *J. Biol. Chem.* **2016**, *291*, 4079–4090. [CrossRef]
20. Wanchoo, A.; Voigt, A.; Sukumaran, S.; Stewart, C.M.; Bhattacharya, I.; Nguyen, C.Q. Single-Cell Analysis Reveals Sexually Dimorphic Repertoires of Interferon-Gamma and Il-17a Producing T Cells in Salivary Glands of Sjogren's Syndrome Mice. *Sci. Rep.* **2017**, *7*, 12512. [CrossRef]

21. Voigt, A.; Gupta, S.; Shen, Y.; Glenton, P.; Li, D.; Ostrov, D.; Bhattacharyya, I.; Nguyen, C.Q. Exploring Mhc Class Ii I-Ab Blockade as a Potential Treatment for Sjögren's Disease in the Mouse Model. *Immunohorizons* **2025**, *9*, vlaf030. [CrossRef]
22. Anaya, J.M.; Mantilla, R.D.; Correa, P.A. Immunogenetics of Primary Sjögren's Syndrome in Colombians. *Semin. Arthritis Rheum.* **2005**, *34*, 735–743. [CrossRef]
23. Nakken, B.; Jonsson, R.; Brokstad, K.A.; Omholt, K.; Nerland, A.H.; Haga, H.J.; Halse, A.K. Associations of Mhc Class Ii Alleles in Norwegian Primary Sjögren's Syndrome Patients: Implications for Development of Autoantibodies to the Ro52 Autoantigen. *Scand. J. Immunol.* **2001**, *54*, 428–433. [CrossRef]
24. Scofield, R.H.; Frank, M.B.; Neas, B.R.; Horowitz, R.M.; Hardgrave, K.L.; Fujisaku, A.; McArthur, R.; Harley, J.B. Cooperative Association of T Cell Beta Receptor and Hla-Dq Alleles in the Production of Anti-Ro in Systemic Lupus Erythematosus. *Clin. Immunol. Immunopathol.* **1994**, *72*, 335–341. [CrossRef]
25. Gupta, S.; Li, D.; Ostrov, D.A.; Nguyen, C.Q. Epitope Mapping of Pathogenic Autoantigens on Sjögren's Syndrome-Susceptible Human Leukocyte Antigens Using in Silico Techniques. *J. Clin. Med.* **2022**, *11*, 1690. [CrossRef]
26. Khan, D.; Dai, R.; Karpuzoglu, E.; Ahmed, S.A. Estrogen Increases, Whereas Il-27 and Ifn-Gamma Decrease, Splenocyte Il-17 Production in Wt Mice. *Eur. J. Immunol.* **2010**, *40*, 2549–2556. [CrossRef]
27. Newcomb, D.C.; Cephus, J.Y.; Boswell, M.G.; Fahrenholz, J.M.; Langley, E.W.; Feldman, A.S.; Zhou, W.; Dulek, D.E.; Goleniewska, K.; Woodward, K.B.; et al. Estrogen and Progesterone Decrease Let-7f Microrna Expression and Increase Il-23/Il-23 Receptor Signaling and Il-17a Production in Patients with Severe Asthma. *J. Allergy Clin. Immunol.* **2015**, *136*, 1025–1034.e11. [CrossRef]
28. Ghisletti, S.; Meda, C.; Maggi, A.; Vegeto, E. 17β-Estradiol Inhibits Inflammatory Gene Expression by Controlling Nf-Kb Intracellular Localization. *Mol. Cell. Biol.* **2005**, *25*, 2957–2968. [CrossRef]
29. Hoffmann, J.P.; Liu, J.A.; Seddu, K.; Klein, S.L. Sex Hormone Signaling and Regulation of Immune Function. *Immunity* **2023**, *56*, 2472–2491. [CrossRef]

Disclaimer/Publisher's Note: The statements, opinions and data contained in all publications are solely those of the individual author(s) and contributor(s) and not of MDPI and/or the editor(s). MDPI and/or the editor(s) disclaim responsibility for any injury to people or property resulting from any ideas, methods, instructions or products referred to in the content.